Canadian Mineralogist
Vol. 16, pp. 547-560 (1978)

THE STRUCTURAL MORPHOLOGY OF OLIVINE. II. A QUANTITATIVE DERIVATION

J. 'T HART*
Geological and Mineralogical Institute, State University of Leiden, Leiden, The Netherlands.

ABSTRACT

The morphology of forsterite (Mg_2SiO_4) is predicted from the crystal structure by quantitative computations of surface energies. Olivines with different compositions will show only small morphological variations. For *F* faces the attachment energies are computed in an electrostatic point-charge model. This is done for three ionic models: Si^{4+}–O^{-2}, Si^{2+}–$O^{1.5}$ and Si^{0}–O^{1-}, representing increasing covalency of the Si–O bonds and increasing amount of preformed SiO_4 tetrahedra. From the attachment energies, taken proportional to the growth velocities, the growth forms for the ionic models are constructed; the resulting habit is always elongated along the *c* axis and slightly tabular on (010). Only small differences in the relative morphological importances of the forms {010}, {110}, {120}, {021}, {001}, {101} and {111} could be observed for the different charge models. The attachment energies computed from Coulomb interactions are considerably reduced when the short-range Born repulsive energies are taken into account. Equilibrium forms are constructed from specific surface energies. As the olivine structure is not completely ionic, the morphology has also been computed for a covalent model: it differs from that of the ionic models by the absence of the {111} and {120} forms. The statistical average morphology observed on natural and artificial crystals lies between the morphologies calculated for the covalent model on the one hand and the ionic Si^{2+}–$O^{1.5-}$ and Si^{0}–O^{1-} models on the other.

SOMMAIRE

On prédit la morphologie de la forsterite Mg_2SiO_4 à partir de la structure cristalline par le calcul quantitatif des énergies superficielles. Des olivines de compositions différentes ne montreront que de faibles variations morphologiques. L'énergie d'attache des faces *F* a été calculée dans un modèle électrostatique à charges ponctuelles. Ces calculs ont été effectués pour une série de trois modèles ioniques Si^{4+}–O^{2-}, Si^{2+}–$O^{1.5-}$ et Si^{0}–O^{1-}, représentant un accroissement de la covalence des liaisons Si–O et du nombre des tétraèdres SiO_4 préformés. A partir d'énergies d'attache, supposées proportionnelles aux vitesses de croissance, on construit les formes de croissance pour les modèles ioniques; le faciès correspondant est toujours allongé suivant *c*, légèrement tabulaire sur (010). Les différents modèles de charges ne produisent guère de différence dans l'importance morphologique relative des formes {010}, {110}, {120}, {021}, {001}, {101} et {111}, Les énergies d'attache calculées à partir des interactions Coulombiques diminuent fortement lorsqu'on prend en considération les énergies répulsives de Born à courte distance. On construit ensuite les formes d'équilibre à partir des énergies superficielles. La structure de l'olivine n'étant pas entièrement ionique, sa morphologie a aussi été calculée pour un modèle covalent : ainsi établie, elle diffère de celle des modèles ioniques par l'absence des formes {111} et {120}. La morphologie moyenne statistique, observée sur cristaux naturels et synthétiques, se situe à mi-chemin entre les morphologies calculées pour le modèle covalent d'une part et les modèles ioniques (Si^{2+}–$O^{1.5-}$ et Si^{0}–O^{1-}) d'autre part.

(Traduit par la Rédaction)

INTRODUCTION

Olivine is a mineral with a highly variable morphology as has been discussed by Goldschmidt (1920), Hintze (1897), Kalb & Koch (1929), Niggli (1927), Niggli & Faesy (1921), Soellner (1911), Zambonini (1900, 1905) and more recently by Bautsch *et al.* (1971), Fleet (1975) and Donaldson (1976). On polyhedral crystals the most commonly observed morphology comprises the forms: {010}, {110}, {021}, {101}, {001}, {111} and {120}. All these crystal forms are *F* faces (faces parallel to at least two *PBC*s: 't Hart 1978). Generally the habit is more or less tabular parallel to the (010) face and elongate along the *c* axis. Atom configurations in the growth layers parallel to these *F* faces, discussed in Part I ('t Hart 1978), are the basis for the computations of surface energies in this paper.

Using the Hartman–Perdok theory, the morphology of crystals from nature or laboratory can be related to structure (Hartman 1973). If observed and predicted morphologies conflict, then this can usually be attributed to special conditions. Concerning these conditions, a few

*Present address: BP Exploration Canada Ltd., 335 8th Avenue S.W., Calgary, Alberta T2P 1C9.

remarks must be made. Crystal habit is strongly affected by degree of supercooling and cooling rate (Donaldson 1976); polyhedral crystals as predicted in this paper may only be expected when these variables are small. The influence of pressure (Abu-Eid & Burns 1976) and of the density and orientations of dislocations can be neglected. Little is known about the influence of impurities on olivine morphology. Kalb & Koch (1929) have tried to attribute the different morphologies to different kind of rocks. However, in going from one rock to another, not only does chemical composition change, but other variables do as well.

We neglect the parameters mentioned above, or assume that they are equal for all crystal faces, whereas growth velocity is assumed to be proportional to the attachment energy (Hartman 1956, 1973). This assumption is only applicable to polyhedral crystals. The attachment energy is the energy released per molecule when a new slice d_{hkl} (a growth layer with thickness d_{hkl}, where hkl satisfies the extinction conditions of the space group) is attached to a crystal face.

The bonds in forsterite are neither purely ionic nor purely covalent. For Mg–O bonds the effective charges are reduced somewhat due to non-Coulombic forces, but for Si–O bonds this effect is considerably higher. For β–SiO_2 Slaughter (1966) computed a covalency of 49%. We may also assume a covalency of about 50% for the Si–O bonds in the olivine structure because they have nearly the same length as in β–SiO_2. To determine the influence of increasing covalency, the crystal morphology of forsterite has been computed for different point-charge models with the following charges on Si and O: Si^{+4}–O^{2-} Si^{2+}–$O^{1.5-}$ and Si^{0}–O^{1-}. This indicates the order of increasing covalency of the Si–O bonds. The crystallizing particles are assumed to be SiO_4^{4-} complexes and Mg^{2+} ions.

The morphology for a broken-bond model has also been computed to examine the influence of increasing covalency on all bonds present. In such a model, it is assumed that interaction only occurs between atoms in the first coordination sphere. The computation of attachment energies in a broken-bond model involves summation of the strengths of all those bonds that will be found per molecule when a new slice is attached to a crystal face. This model is considered as completely covalent. The differences between the covalent, partly ionic and ionic models will be discussed.

The Computation of Attachment Energies in the Ionic Model

The significance of the attachment energy as a measure of growth velocity in kinetic theories such as the *BCF* theory and computer simulations is given by Bennema & Gilmer (1973). When growth takes place, there is more or less a state of disequilibrium, so that in nature, we shall always observe the growth habit and not the equilibrium habit.

As mentioned above, attachment energies are assumed to be a measure of the growth velocities of F faces. Faces with high growth-velocities (*i.e.*, with high E_{att}) will disappear from the growing crystal. The growth form has been constructed by plotting the growth rates along the normals to the various faces. In our case, where only F faces are involved, layer growth is the growth mechanism. This means that we have either two-dimensional nucleation or spiral growth. We define E_{sl} as the energy necessary for the formation of a new growth slice, released per molecule when a new slice d_{hkl} is formed. E_{sl} and E_{att} are complementary and related by

$$E_{cr} = E_{sl} + E_{att} \tag{1}$$

where E_{cr} is defined as the crystal energy; E_{cr} is equal to be sublimation energy when the crystal grows from vapor. We can compute these energies if we consider the atoms as point charges. In this case we can use the Madelung method (Madelung 1918, Kleber 1939, Hartman & Perdok 1955, Hartman 1973) for calculating the electrostatic potentials.

The structure has been divided into a set of parallel *PBC*s (n, m), where m is the number of the slice and n the number of the *PBC* within the slice (Fig. 1a). Each *PBC* (Fig. 1b) has been divided into a set of rows through the different ions parallel to the direction of the *PBC*. According to Hartman (1973), the potential at a point P_j having coordinates x_j and r_j, where the x axis is parallel to the *PBC* direction and r_j is the distance of P_j from the row of ions at which the potential is computed, is, for x_j and $r_j \neq 0$ (P_1 in Fig. 1b, c),

$$V_j(r,x) = \frac{2 z_j e}{p} \left[\sum_{l=1}^{\infty} \pi i H_0^{(1)} \left(\frac{2\pi i l r_j}{p}\right) \cos\left(\frac{2\pi l x_j}{p}\right) + \ln\frac{2p}{r_j} + \ln N \right] \tag{2}$$

where $iH_0^{(1)}$ $(2\pi i l r_j/p)$ is the Hankel function of zero order, with argument $(2\pi i l r_j/p)$ as tabulated by Jahnke & Emde (1960). We could consider, through every ion of the *PBC*, a row of $2N$ equally spaced point-charges, in the direction of the *PBC*, with period p and charge $z_j e$.

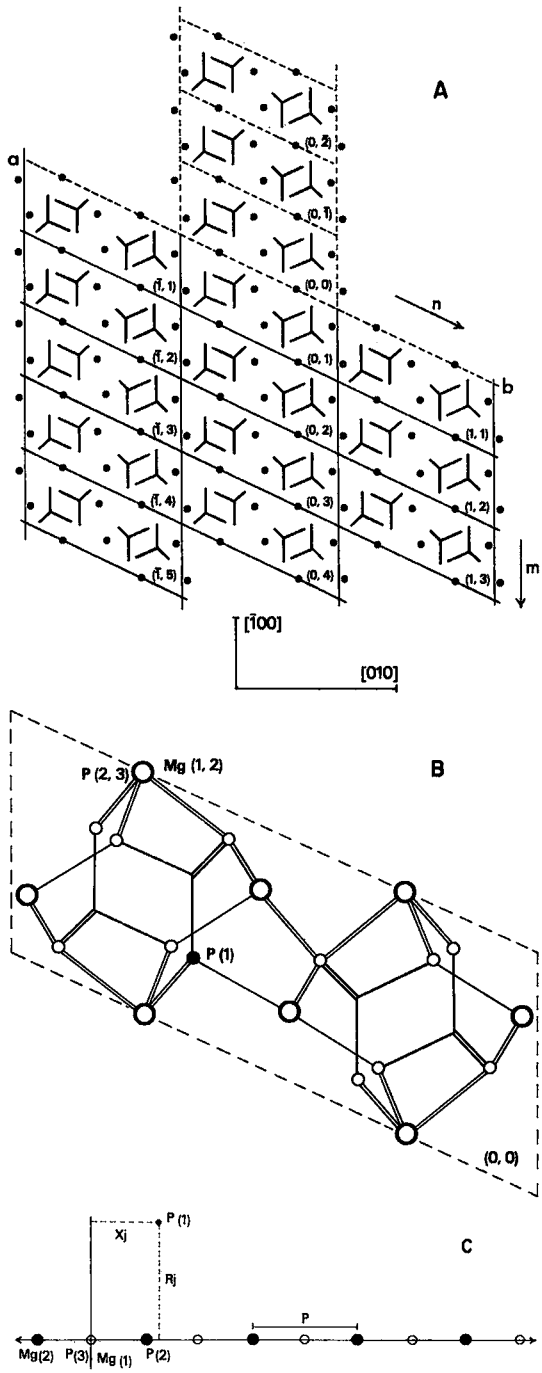

FIG. 1. (a) Schematic drawing of *PBC*s parallel to [001], within the $d_{1\bar{1}0}$ slice of olivine. The chains (n,m) are labeled. (b) The *PBC* (0,0) (Fig. 1a), showing the three different positions of P at which the potential due to a row of Mg(1) ions may be computed. (c) An infinite row of Mg(1) ions perpendicular to the plane of b. For the computation of the potential at a point P_j due to a row Mg(1) ions, there are different positions, P_1, P_2 and P_3. P_1 can represent any ion of the *PBC* outside the row, in which case eq. (2) has to be applied. Formula (3) is applied for the potential at a point P_2 in the row but not situated on a Mg(1) ion, so $r_j = 0$. Formula (4) is used to compute the potential at a Mg(1) site, P_3.

The value of r_j is mostly different from zero, so that eq. (2) can usually be applied. When P_j (P_2) is situated on a row of non-identical ions $P(3)$ (see Fig. 1c), then $x_j \neq 0$ but $r_j = 0$ (Fig. 1b, c), and the formula becomes

$$V_j(0,x) = -\frac{z_j e}{p}\left[\psi\left(\frac{x_j}{p}\right) + \psi\left(1 - \frac{x_j}{p}\right) - \frac{p}{x_j} - \frac{p}{p - x_j}\right] + \frac{2z_j e}{p} \ln N \qquad (3)$$

where $\psi(y) = d\ln y!/dy$. There is a third possibility where P_j is situated at the position of a point charge in the row. Then the potential at P_j (P_3) due to that row has to be computed for $x_j = 0$ and $r_j = 0$ according to

$$V_j(0,0) = \frac{2\,z_j e}{p}[C + \ln N] \qquad (4)$$

$C = -\psi(0) = 0.577216$ (Euler's constant).

The potential at a point P_j due to the kth row within a *PBC* (0,0) is V_{jk}. To obtain the potential at a point P_j due to the whole *PBC* (0,0) we have to sum the potentials due to all the rows within the *PBC*

$$V_j = \sum_{k=1}^{K} V_{jk} \qquad (5)$$

where K is the number of rows. The energy is computed by multiplying the potential by the charge $z_j e$. The energy per molecule to form a *PBC* (0,0), E_{ch} is

$$E_{ch} = \frac{1}{2}\sum_{j}^{J}\sum_{k}^{K} z_j e\, V_{jk} \qquad (6)$$

where J is the number of ions per period in one *PBC*. If through every ion j we can have a row, $K=J$. The energy E_{sl} is the energy necessary per molecule to form a growth layer of thickness d_{hkl}. Not only is the interactive energy within the *PBC* (0,0) considered, but also with the neighboring *PBC*s within the zero slice.

$$E_{sl} = \frac{1}{2}\sum_{n=-\infty}^{+\infty}\sum_{j=1}^{J}\sum_{k=1}^{K} z_j e V_{njk} \qquad (7)$$

where n is the serial number of the *PBC* within the slice. To obtain the total interaction energies of one molecule with all *PBC*s within the slice, we have to sum from $-\infty$ to $+\infty$ (Fig. 1a). In these cases formula (2) is always applied, because $r_j \neq 0$. The contribution of the first term of formula (2), the Hankel function, rapidly decreases and is shown to be convergent (Kleber 1939). However, the contribution of the second part of the formula converges very slowly. To that end a power series was developed (Hartman 1956, Woensdregt *in prep.*).

The attachment energy was computed as follows from the potentials V_{mnjk}:

$$E_{att} = \sum_{m=1}^{+\infty} \sum_{n=-\infty}^{+\infty} \Sigma_j \Sigma_k z_j e V_{mnjk} \qquad (8)$$

If E_m represents the interaction energy, per molecule, of a *PBC* with the mth slice ($m = 0, 1, 2, \ldots, M$), then $E_{sl} = E_0$ and $E_{att} = \sum_{m=1}^{+\infty} E_m$.

The computations of the potentials, based on formulae (2–4), have been done with a Fortran IV programme called ENERGY (Woensdregt 1971).

The morphology of olivine is derived from the structure of the Mg end-member forsterite (Mg_2SiO_4), with space group *Pbnm* and $Z=4$. The cell constants and atomic parameters were determined by Birle *et al.* (1968) and listed in 't Hart (1978, Table 1).

Results

The growth form (ionic model)

The ionic growth form is determined from the attachment energies, computed in the way explained above. High attachment-energy means high growth-velocity of the crystal in the direction perpendicular to the face considered.

The theoretical models of growth forms of forsterite are constructed by Wulff's method (1901). The central distance of each crystal face is proportional to the attachment energy of the face. "Wulff plots" parallel to zones of strong *PBC*s are made. In each plot the crystal is bounded by faces with the lowest attachment energies. The region of the Wulff plot that can be reached from the origin without crossing any growth surface belongs to the crystal. One Wulff plot of the Si^{4+}–O^{2-} and Si^{0}–O^{1-} models parallel to the [001] direction is shown (Fig. 2). From Wulff plots in different directions it is possible to construct a three-dimensional drawing of the crystal. The coordinates of the vertices were obtained with a computer program. The orthographic crystal drawings, made by the program CRYSTAL-DRAW (Strom 1977), are projections of the crystal in the [621] direction of the cubic system onto the cubic $(\bar{6}2\bar{1})$ plane and the crystals are of equal volumes.

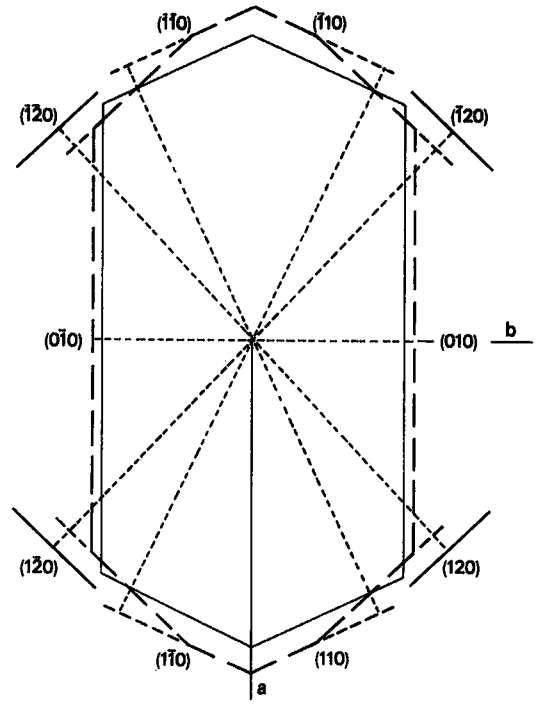

FIG. 2. The change due to increasing covalency of the Si–O bonds is shown in a Wulff plot // [001] of the ionic growth form of olivine, corrected for a realistic Mg distribution. Continuous line, model I; dashed lines, model III.

As already mentioned, the attachment energies are computed for three different charge models: (I) *The Si^{4+}–O^{2-}* pure ionic model. In this and the other two models, the SiO_4 tetrahedra are considered as complete crystallization units, in such a way that no Si–O bonds are broken. All the ions have maximum charges; in reality, however, the effective charges should be lower (Fleet 1974). (II) *The Si^{2+}–$O^{1.5-}$ model.* According to Born (1964), this model is energetically the most favorable. Owing to charge reduction of the SiO_4 tetrahedron, the bonding within this tetrahedron is less ionic, and partial covalency (50%) is introduced. The Mg–O bonding remains purely ionic, but the bond strength decreases owing to the de-

TABLE 1. ENERGIES FOR THE MODELS I, II AND III (IN KCAL/MOL)

Face	E_{att}			E_{cor}	E^{d}_{att}			E_{rep}	E^{H}_{att}			E^{o}_{cov}
	I	II	III		I	II	III		I	II	III	
(010)	-129.92	-130.21	-138.47	0	-129.92	-130.21	-138.47	79.10	-50.82	-51.11	-59.37	0.780
(110)*	-323.26	-291.34	-259.76	0	-323.26	-291.34	-259.76	197.00	-126.26	-94.34	-62.76	1.491
(110)+	-394.35	-401.43	-415.18	-155.73	-238.62	-245.57	-259.45	150.19	-88.43	-95.38	-109.26	1.380
(120)	-324.54	-312.51	-305.39	-77.57	-246.97	-234.94	-227.82	177.07	-69.90	-57.87	-50.75	1.406
(021)	-338.65	-314.29	-289.05	-49.92	-288.73	-264.37	-239.13	128.67	-160.06	-135.70	-110.46	1.217
(111)	-395.57	-383.23	-372.49	-42.70	-352.87	-340.53	-329.79	204.06	-148.81	-236.47	-125.73	1.736
(112)	-406.55	-372.37	-338.51	0	-406.55	-372.37	-338.51	216.93	-189.62	-155.44	-121.58	1.983
(101)	-411.65	-392.89	-374.63	-46.83	-364.82	-346.06	-327.80	177.16	-187.66	-168.90	-150.64	1.465
(130)	-424.87	-389.42	-355.30	0	-424.87	-389.42	-355.30	216.20	-208.67	-173.22	-139.10	1.746
(121)	-443.61	-432.95	-426.87	-43.52	-400.09	-389.43	-383.35	208.24	-191.85	-181.19	-175.11	1.831
(132)	-457.41	-421.96	-386.80	0	-457.41	-421.96	-386.80	251.63	-205.78	-170.33	-135.17	2.102
(001)	-471.81	-436.10	-396.55	-129.71	-342.10	-306.39	-266.84	190.59	-151.51	-115.80	-76.25	1.702

* Values for the d_{110} slice with no Mg ions at the slice boundary; + values for the d_{110} slice with Mg ions at the slice boundary; o broken-bond strength for the covalent model, in valence units.

creased oxygen charges. (III) *The Si^0–O^{1-} model.* Here the silicon ion has no charge and the whole tetrahedron is considered as a covalently bonded group with charge –4. This means that the electrostatic energy is further reduced. The model assumes that (a) all the SiO_4 tetrahedra are covalently-bonded preformed building units; (b) the Mg–O bonds remain completely ionic.

We may present the model in this way, because no Si–O bonds have been broken. Presumably the charges of the SiO_4^{4-} tetrahedra in model II are the most realistic.

The configurations of the ions within the slices are fixed by the composition and orientation of the *PBC*s ('t Hart 1978). For all three models the same *PBC*s have been used. In presenting the various energies for models I, II and III (Table 1) for each *F* face, we give the attachment energy E_{att} in kcal/mol. More detailed data are available in Tables 2, 3 and 4, in which are given in addition, the slice energy E_{sl} and the contributions of the slices 1, 2, *etc.*, by E_1, E_2,*etc.*; Tables 2, 3 and 4 available at nominal cost from the Depository of Unpublished Data, CISTI, National Research Council of Canada, Ottawa, Ontario K1A 0S2, Canada. At a point P_j the contribution to the attachment energy of the slice $(n+1)$ is neglected if the contribution of the nth slice is smaller than 0.004 kcal/mol.

With the exception of the *PBC* within the $d_{11\bar{1}}$ slice, the slices and *PBC*s that give the lowest attachment energies are drawn in Figures 2 to 5 of 't Hart (1978). It was not possible to decide on the basis of qualitative considerations which *PBC* configuration within the $d_{11\bar{1}}$ slice is energetically the most stable. For the configuration of the $d_{11\bar{1}}$ slice (see also Fig. 4, 't Hart 1978), the attachment energy was found to be –493.25 kcal/mol for model I. However, if the slice was translated over a distance $\frac{1}{2}d_{111}$, then the attachment energy for the same model became –395.57 kcal/mol. Therefore, the latter modified configuration of the slice is much more stable.

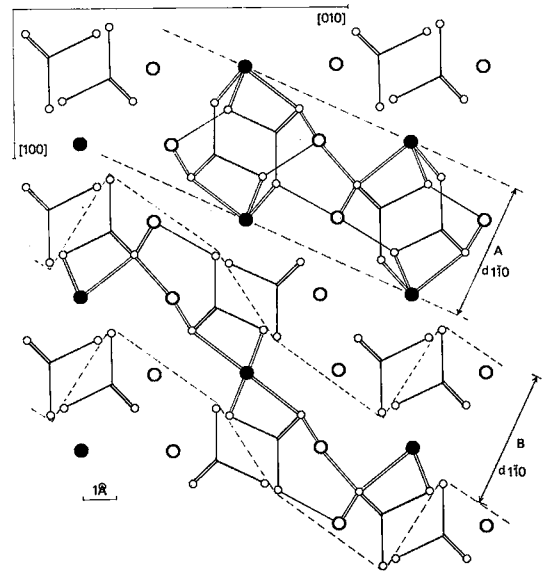

FIG. 3. The two different configurations of the d_{110} slice: *A* with the flat surface and all the Mg ions in M(I) positions at the slice boundary, *B* with the undulating surface and no M(I) positions at the slice surface.

The d_{110} slice could be formed using two different *PBC*s, *A* and *B* (Fig. 3). The *B* configuration gives the slice an undulating surface and the attachment energy for this configuration in model I is –323.26 kcal/mol. The *A* configuration of the d_{110} slice has all the Mg ions in M(I) positions at the geometric boundary of the slice. The attachment energy for this slice in the same model is –394.35 kcal/mol. Below we shall see the difference between these two slices.

For model I, the lattice energy E_{cr} is –5760.37± 0.20 kcal/mol. The lattice energies

for models II and III with the reduced charges are $-2982.59\pm$ 0.34 kcal/mol and $-1455.69\pm$ 0.40 kcal/mol, respectively.

The computation of slice (E_{sl}) and attachment energies (E_{att}) is based on the assumption that a *PBC* does not have a dipole moment perpendicular to the *PBC* direction. The consequence of this symmetry is that the M(I) Mg ions, located at symmetry centres, occur at the geometric slice boundaries. Therefore, such an ion and its charge are equally divided between the two adjacent slices. This leads to a surface structure having a statistical distribution of the Mg ions between the two slice boundaries. However, it is very likely that in reality these Mg ions at the surface are ordered in some way we shall call a realistic distribution. Yet the statistical distribution is a necessary step to obtain attachment energies for the realistic model. It is easy to compute a correction energy to obtain the attachment energy for the realistic distribution from a model with a statistical distribution. A direct calculation of the attachment energy for a realistic contribution would increase the necessary computation time by at least a factor of 2 or 4. This is due to the fact that a *PBC* with a realistic distribution has a period twice as long as the lattice period, because every second Mg ion in a row is missing. The same applies for the translation in other directions, so that two adjacent *PBC*s of double period must be combined to form one huge ionic chain with four times as many atoms as usual. It is much more convenient to compute correction energies as shown in the next paragraph.

Correction Energy for a Realistic Distribution of Mg Ions at the Boundaries of Slices

Giese (1974) pointed out the energy correction for a realistic distribution of ions by the computation of surface energies on cleavage planes of muscovite. This correction seems reasonable although we do not have a cleavage surface here but the surface of a growing crystal. The correction energies can also be computed with the program ENERGY in the following way (P. Hartman, pers. comm.). Suppose for example that there are two ions per unit cell at a geometric slice boundary (Fig. 4). In the case of a statistical distribution all the Mg ions have a charge +1, because they are divided between the two adjacent slices. For a realistic distribution, only one position on the geometric slice boundary per unit cell (position I in Fig. 4), will be occupied

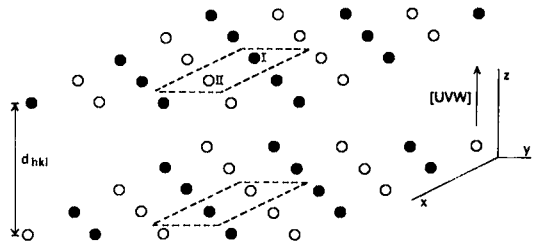

FIG. 4. Identical Mg ions on the boundary surfaces of a slice d_{hkl}. The identical lattice translation from slice to slice is [**uvw**]. One mesh area is indicated. For computation of the correction energy, the translations within the slice have to be chosen in such a way that a lattice plane is formed with alternating occupied and unoccupied Mg positions.

by Mg^{2+} ions. Now the correction energy is computed by adding an ion of charge +1 in position I (Fig. 4) and an ion of charge −1 in position II. This means that if the correction is applied to a model with a statistical distribution of +1 charges on the geometrical boundary, all the ions in position I will get a charge +2 and in position II a charge 0. The vector [**uvw**] is the translation from one slice to the next. The ions translated from the upper slice boundary to the lower boundary have opposite charges. Owing to the symmetry and the opposite charges of these identical ions, the total sum of interaction energies with the rest of the ions within the slices is zero. Thus, for the computation of the attachment energies, only the interaction energies between the Mg ions at the geometric slice boundaries need be considered.

If we lower the E_{sl} by the correction energy, the interaction between arrays of alternating charged Mg ions on both sides of the slice, we will get the same E_{sl} energy as computed with Mg^{2+} ions in only half the M(I) positions at the geometric boundaries. The E_{sl} energy becomes more negative because the Mg^{2+}–Mg^{2+} interaction decreases. This results in a less negative attachment energy (eq. 1).

The Mg^{2+}–Mg^{2+} interaction energy is the same for all three models, because the charge of the Mg ions is the same. So the correction energies may be used to correct the attachment energies of all three models (Table 1). There are five slices of F faces without Mg ions at their boundaries, (010), (112), (130), (132) and (110) with the undulated surface, so their attachment energies are not corrected. These crystal forms become relatively less important (Figs. 5a–c).

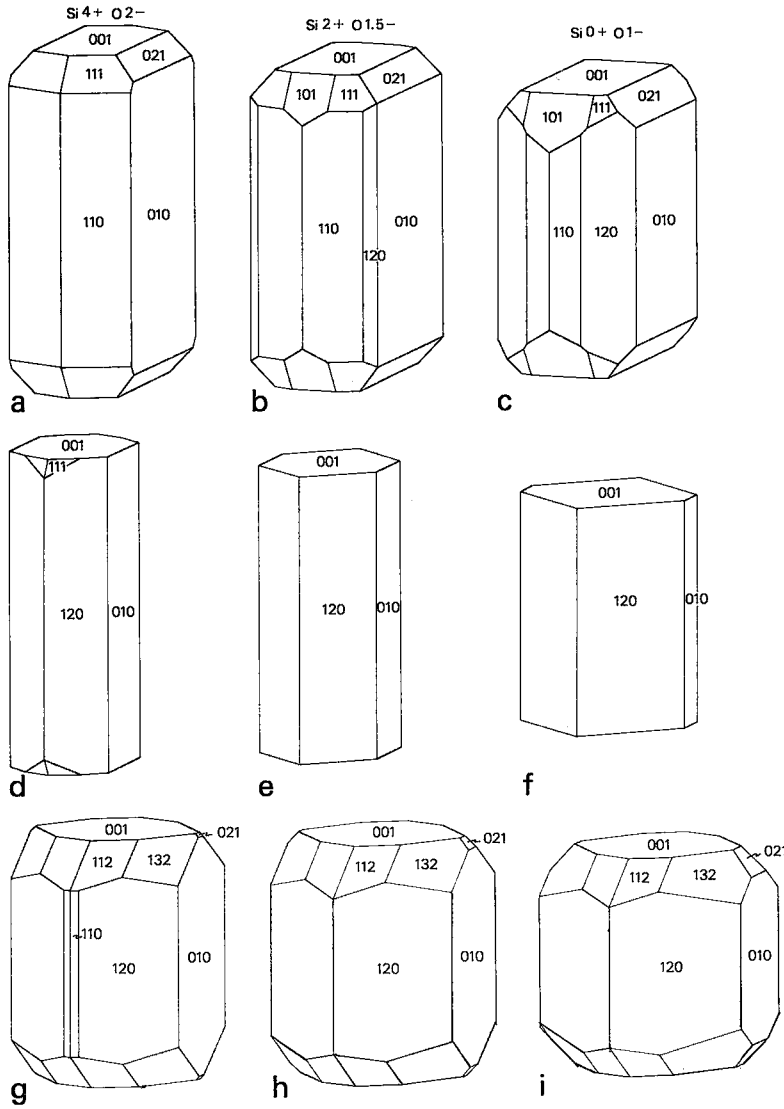

FIG. 5. Growth forms of olivine for the three different charge models; a–c, growth forms of models with a realistic distribution of Mg ions at the slice boundaries; d–f, growth forms corrected for both a realistic distribution of the Mg ions and for the Born repulsion energy; g–i, equilibrium forms of olivine (realistic Mg distribution).

As has already been mentioned above, there are two different configurations of the $d_{1\bar{1}0}$ slice (Fig. 3). For the undulating $d_{1\bar{1}0}$ slice without Mg ions on the slice surface (E_{att}=−323.26 kcal/mol), no correction for a realistic distribution has to be computed. However, for the other configuration of the slice, with the flat surface and all the Mg ions in M(I) positions at the geometric slice boundary, the correction energy E_{cor}=−155.73 kcal/mol has been computed. The attachment energy for this configuration of the slice is −394.35−(−155.73)=−238.64 kcal/mol (model I); for a realistic Mg distribution this slice is the most stable one.

THE BORN REPULSION ENERGY

Until now only Coulomb interactions have been considered, giving rise to the most important electrostatic energy in ionic crystals.

However, especially with respect to the attachment energy, the Born repulsive interaction can be an important contribution. Computations of the Born repulsive energy (Appendix) show, for the [001] zone, contributions to the attachment energy between 60–70%, and for the other faces in between, 45–58% (Tables 1-4). In all three models, this fact is clearly responsible for the reduction in richness in crystal forms (Figs. 5d–f).

The Growth Form (Covalent Model)

Besides the ionic and partly ionic models, now a covalent model is introduced. The covalent case is represented by a broken-bond model in which the bond strength for each bond has been taken into account. There are two different bond types (Mg–O and Si–O) in the structure; these are of different bond strengths. For that reason, the bond strengths were computed according to Brown & Shannon (1973) and Povarennykh (1972). The bond strengths were expressed in different units, but the ratios between them are about the same. For further calculations the values of Brown & Shannon are used.

For all the *F* faces the number of broken Mg–O bonds per molecule per mesh area are given in Table 5 (deposited with Tables 2, 3 and 4). These bonds have already been shown in Figures 2 to 5 of 't Hart (1978) as dotted lines. The bond strengths must be summed over all the broken bonds per mesh area and divided by the number of molecules per mesh. This broken-bond strength per molecule (Table 1) is assumed to be a measure of the growth velocity of the faces and is equal for both a statistical and a realistic distribution, because the number of broken bonds remains equal.

We could construct the $d_{1\bar{1}0}$ slice in two different ways ('t Hart 1978). Both have 18 broken bonds per mesh area, that is, 4.5 broken bonds per molecule. The total broken-bond strength per molecule for the d_{110} slice is 5.520 *v.u.* (valence units) for the flat slice and 5.964 *v.u.* for the slice with the undulating surface.

The broken-bond model (Fig. 6) is of a form slightly less elongate parallel to the *c* axis than the ionic growth forms. If we compare the broken-bond model with the ionic models, which were not corrected for the repulsion energy, we find good agreement. With the exception of the {120} form, which does not occur in the covalent model, the tendency of the changing morphology from I to III continues for the covalent model. As we can see,

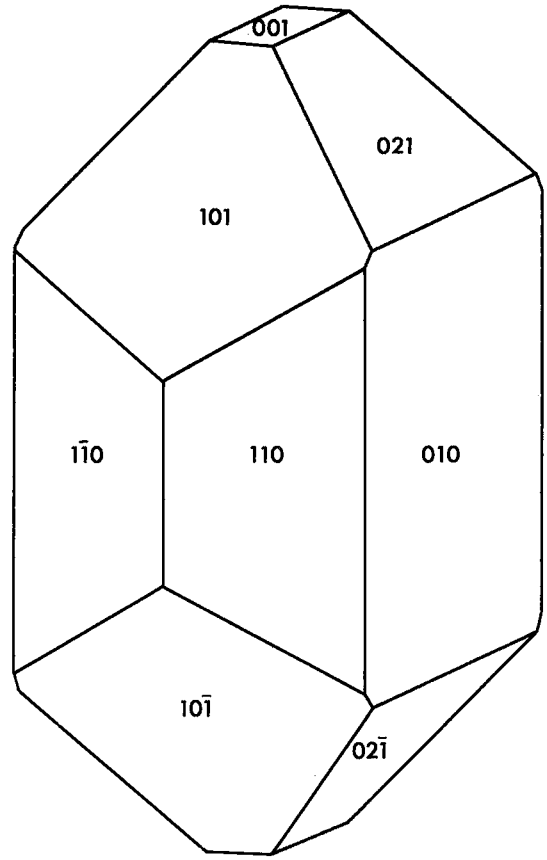

FIG. 6. Growth form for broken-bond model.

{101} and {021} become more important, {111} becomes less important, and the crystal becomes less elongate along [001].

The Equilibrium Form

Besides growth forms, a theoretical equilibrium morphology has been computed from the specific surface energies. The equilibrium form of a crystal is defined as the one that has the minimum value for the total surface-free-energy at constant temperature and crystal volume.

The specific surface-free-energy γ is the energy per unit of surface to divide an infinite crystal in two halves along a specified surface. Instead of the free energy we will calculate the energy that can be computed from the contributions of different slices to the attachment energies. If for example we consider a suite of slices, then the number of cells per cm^2 is $1/M_{hkl} = d_{hkl}/V_p$ (V_p is the volume of the primitive cell) and the number of molecules is $Z_p \cdot d_{hkl}/V_p$ (Z_p is the number of molecules per

primitive cell). The interaction energy between two slices per molecule is E_m ($E_1 \ldots E_8$, Tables 2–4, deposited) and the total interaction energy between the suites of slices of the divided two infinite half-crystals is

$$E_s = \sum_{m=1}^{+\infty} mE_m$$

For example, in the case of the d_{110} slice, we assume that the crystal is divided along *ab* (Fig. 1a). Then the interaction per molecule between slice 0 and the suite of slices, E_m ($m = 1,2,\ldots\infty$), is computed in *PBC* (0,0). In the same way the interaction per molecule between the slice −1 and the suite of slices is computed as the interaction of *PBC* (0,−1) with the same suite of slices. This interaction energy with the slice 1, 2, 3, ... is the same as the interaction per molecule in *PBC* (0,0) with the slices 2, 3, 4, ..., which explains the above given summation. The total interaction now is computed per 2 cm², so we have to divide by 2, and we find for the specific surface energy (Hartman 1974):

$$\gamma = f Z_p d_{hkl} E_s / 2V_p \qquad (9)$$

where f=695.1904 is a conversion factor to obtain γ in erg/cm² from E_s in kcal/mol.

To compute γ for the models with a realistic distribution on the crystal surface, one should know the contributions E_m of the single slices for these corrected models. The corrections that were computed for a realistic distribution of Mg ions are completely contributed by E_{s1} and E_1. To know the contributions of the corrected model to E_1, one should take for the computation of attachment energies such a number of molecules that after translation within the slice in both translation directions, there are at least one vacant and one identical occupied Mg site. Such computations were not carried out, owing to long computing times. Because E_{cr} stays constant, $E'_1 = E_1 - E_{cor}$ and $E_{s1} = E'_{s1} + E_{cor}$.

If we construct the equilibrium morphologies from the specific surface energies computed for a realistic Mg distribution (Table 6), then in addition to {010}, {120}, {001}, {110} and {021}, the {112} and {132} forms appear. From model I to model III (Fig. 5g–i), the crystal habit becomes less elongate parallel to the *c* axis. The {110} form is present only in model I, and the importance of the {120} and {021} forms increases.

Discussion

In the models presented here an attempt was made to predict the morphology of forsterite on the basis of electrostatic forces for the ionic model, and on the basis of bond strengths for the covalent model. In all models the SiO_4 tetrahedron is assumed to exist as a precrystallization unit, because it probably exists at temperatures at which forsterite crystallizes. Therefore, during crystallization only Mg–O bonds have to be formed. It has been assumed that the growth velocities in the directions normal to the faces are determined by layer-growth mechanisms, because all the faces here considered are *F* faces. For that reason the attachment energies, assumed proportional to the growth velocities, are computed for the ionic models.

Now let us consider the predicted habits. In the models that are corrected for a realistic Mg distribution, we see that {101}, which does not occur in model I, becomes more important with increasing covalency of the Si–O bonds. We observe the same effect for the {120} form,

TABLE 6. E_S AND THE SPECIFIC SURFACE ENERGIES γ FOR A REALISTIC Mg DISTRIBUTION ON THE SLICE SURFACES FOR THE THREE IONIC MODELS

	Si^{4+}		Si^{2+}		Si^{0}	
Face	E_S	γ	E_S	γ	E_S	γ
(010)	−129.77	−3160.62	−130.28	−3173.04	−139.34	−3393.70
(110)*	−324.93	−6682.14	−292.23	−6009.68	−260.46	−5356.33
(110)†	−394.17	−4903.49	−401.74	−5059.17	−415.78	−5347.90
(120)	−322.09	−4059.12	−308.26	−3829.53	−299.42	−3682.79
(021)	−336.56	−5311.64	−312.28	−4861.71	−287.14	−4395.85
(111)	−388.06	−5763.21	−377.11	−5580.48	−367.89	−5426.62
(112)	−455.99	−5347.98	−419.54	−4920.49	−385.71	−4523.72
(101)	−428.09	−6772.22	−409.58	−6443.44	−391.85	−6128.50
(130)	−408.73	−5396.68	−370.52	−4892.17	−338.53	−4469.79
(121)	−492.85	−6448.47	−480.76	−6274.96	−474.91	−6191.01
(132)	−519.91	−5039.88	−477.33	−4627.12	−438.10	−4246.84
(001)	−453.67	−4625.33	−421.84	−4170.88	−384.79	−3642.75

*, †: see Table 1.

also not important in the completely ionic model, but in model III it is more important than the {110} form, whereas {111} and {010} become slightly less important. In summary we may say that with increasing covalency of the Si–O bonds and with decreasing Coulomb energy of these bonds, the crystal habit becomes a bit less tabular parallel to (010) and less elongate parallel to the *c* axis.

Comparing the habit of the covalent broken-bond model (Fig. 6) with model III having the realistic Mg distribution (Fig. 5c), we observe a change toward equidimensionality. The {111} form, that became gradually less important, has disappeared and {101} and {021} have become more important. The only disagreement between model III and the covalent model is the absence of the {120} form in the latter. In this model the {110} form is favored by the short-range interaction of the covalent Mg–O bond.

The influence of the repulsion energy on the attachment energy should now be discussed. Those faces having, per molecule, many dangling Mg–O and O–O contacts at the surface, give a high contribution to the repulsion energy. This means that slices with low d_{hkl} values and in general high attachment energies largely contribute to the repulsion energy. However, we cannot say that crystal faces with low d_{hkl} values become relatively more important when the Born repulsion energy has been taken into account. Their growth velocities are reduced even by slightly smaller percentages, which leads to more simple morphologies (Fig. 5d–f). So one may check in this model the extent to which the correction arising from the repulsion energy is reliable.

The morphologies of the three models are elongate along the *c* axis if the repulsion energy is assumed to be attributed to nearest-neighbor interaction. The elongation along the *c* axis of crystal drawing shows that this method has to be more refined and that presumably also other phenomena have to be taken into account, such as quantum-mechanical interactions (Lombardi & Jansen 1966) and surface distortion (Verwey 1946).

The equilibrium forms are more equidimensional than the other models. In addition to {010}, {120}, {001}, {021} and {110} (only model I), the {112} and {132} forms are present. This is the most important difference between these and most of the other models. The {112} form is only observed on crystals from pallasitic meteorites (Goldschmidt 1920), but never on terrestrial crystals. The presence of {112} and the equidimensional habit of crystals from these meteorites indicate a more or less equilibrium habit. This is also asserted by Scott (1977), who assumed that equilibrium forms of olivines in pallasitic meteorites are due to a diffusion process having, as driving force, the difference in surface tension between olivine and the metal melt. The {132} form seems not to have been recorded in the literature.

Let us compare the morphologies computed for the different models with that of olivine crystals from nature. These include not only the Mg end-member forsterite but also olivine crystals in which magnesium has been replaced to a smaller or larger extent by iron. Due to the richness of crystal forms of olivine crystals in nature, it is not possible to make a comparison with a single type. But we can look at a number of special criteria like combinations of forms, "Fundortpersistenz" (Niggli 1941) and overall statistical appearance of the different crystal forms. Kalb & Koch (1929) distinguished three different occurrences: basaltic lavas, contact metamorphic calcareous rocks and cavities. Of course, there are more kinds of rocks in which olivine crystals could be found, but owing to the lack of descriptions of those rocks we are limited to the above three types. Olivine crystals from basaltic lavas (*e.g.*, tephroite or limburgite) are commonly described. Percentages of the occurrence of crystal forms (Table 7, column I) for 171 crystals from a limburgite from Sasbach, Kaiserstuhl, are given by Kalb & Koch (1929). The most frequently observed combination of forms was {010}, {110}, {021}, but {120}, {101}, {111} and {001} were also rather commonly observed. The same combination of forms was observed on olivine crystals from the Vesuvius latites and tephroites (Goldschmidt 1920, Hintze 1897). The proportion (in %) of different forms on crystals of

TABLE 7. IMPORTANCE OF CRYSTAL FORMS, IN PERCENTAGES, BASED ON THE PRESENCE OF FORMS

Face	I	II	III
(010)	94.2	100.0	91.7
(110)	76.1	96.8	79.1
(021)	79.6	74.2	79.1
(111)	67.3	90.3	68.1
(120)	62.6	38.7	57.7
(101)	52.1	51.6	53.3
(001)	47.4	38.7	47.7
(100)	38.0	19.4	35.7
(011)	28.7	19.4	30.7
(121)	23.4	19.4	26.3
(130)	14.6	19.4	14.7
(131)	8.2	-	8.2

I: Occurrence of crystal forms on 171 olivine crystals from volcanic rocks of the Sasbach type (Kalb & Koch 1929); II: "Fundortpersistenz" of olivine crystals from Vesuvian basalts; III: occurrence of crystal forms of olivine crystals according to Goldschmidt's *Atlas der Krystallformen* (1920).

Vesuvian basalts (Table 7, column II) shows very good agreement with crystals of the Sasbach type (column I). More recently Brothers (1959) described olivine crystals from a porphyritic alkali basalt having the forms {010}, {110}, {101}, {021} and occasionally {120}. Many others have given descriptions of olivine crystals from basaltic rocks, with almost always the same basic morphology: {010}, {110}, {021}, whereas {120}, {101}, {001} and {111} are also rather common.

However, for most crystals described in the early literature, the host rock was poorly known or completely unknown; chemical analyses were given in only a very few cases. For that reason the influence of single impurities on the morphology remains to be studied ('t Hart *in prep.*).

The olivine crystals from basaltic rocks may well be compared with the models of Figures 5b, c. This means that the growth process represents in nature a situation in which the SiO_4 groups are preformed crystallizing particles, and the Si–O bonds are at least 50% covalent. The repulsion energy must not be neglected, but it must be considered with caution.

Olivine crystals from calcareous contact metamorphic rocks, with a composition of forsterite or monticellite ($CaMgSiO_4$), show greater richness of forms. A few of these crystals from near Monzoni in Tirol (Goldschmidt 1920) always show {010}, {111} and {120} as the most important forms; {110}, {021}, {121} and {101} are common, whereas {011} is occasionally observed. These crystals are equidimensional.

Crystals, generally fayalite-rich, grown from silica-bearing aqueous solutions in cavities, mostly show a habit that compares well with that of olivine crystals in contact metamorphic calcareous rocks (Kalb & Koch 1929).

If we look at the crystal forms drawn in the "Atlas der Krystallformen" (Goldschmidt 1920), we observe also that the crystal forms already mentioned are statistically the most important ones (Table 7, column III). There is also good agreement between predicted morphology and the morphology of artificial olivine crystals. Artificial cobalt olivine crystals are elongate parallel to [001], the {110} form being dominant; in addition, {010}, {021}, {101}, {111}, {121}, {001}, and sometimes {131} and {211} are recorded ('t Hart & Wessicken 1977). Forsterite grown in a MoO–Li_2O–V_2O_5 flux (Vu Tien *et al.* 1972) shows the forms {110}, {010}, {101}, {021} and {001}, whereas the crystals are less elongate along the *c* axis. More V_2O_5 favors the {110} form. From the same flux, but with an abundance of MgO, crystals with the same forms as above been grown, but then with the form {120} always present in addition ('t Hart *in prep.*).

Conclusions

1. According to attachment-energy calculations, the growth form (ionic model) with a realistic Mg distribution on the boundaries of the slices is bounded by the forms: {010}, {110}, {111}, {021}, {001}, and moreover by {101} and {120}. The latter two forms are absent in model I. By introducing increasing covalency of the Si–O bonds, these forms become more important and the crystal becomes less elongate parallel to [001].
2. Correction of the ionic growth forms for the Born repulsion energy reduces the number of crystal forms to {120}, {010}, {001}, whereas {111} only is present in model I.
3. The equilibrium form is less elongate along [001] and more equidimensional. The theoretical equilibrium form is defined by {120}, {010}, {001}, {021}, {112} {132} and {110}. The last form is only present in model I.
4. The morphology of the covalent broken-bond model consists of the forms {010}, {110}, {101}, {021} and {001}.
5. The statistically most important forms on crystals from nature are {010}, {110}, {001}, {021} and {101}; {120} and {111} are also commonly observed.
6. Olivine crystals from pallasitic meteorites agree rather well with the theoretical equilibrium habit. They are equidimensional and are the only crystals known to show the {112} form; the {120} form is less pronounced than in the predicted habit.
7. The most satisfactory model for crystals from nature lies between the covalent broken-bond model and an ionic one intermediate between model II and III, corrected for a realistic Mg distribution. This agrees with Born (1964), who found model II to be energeticaly the most favorable configuration. A contribution for the Born repulsion energy was computed, but from the discrepancy in morphology between the models corrected for the Born repulsion energy on one hand and crystals from nature on the other, it may be concluded that these models have to be further refined.

Acknowledgements

The author is greatly indebted to Professor P. Hartman for his advice, for his many stimulating discussions and his criticism of the manuscript. I would like to acknowledge Drs. C.F. Woensdregt for his critical reading of the

manuscript and for use of the computer program ENERGY. I would also like to thank Dr. P. Bennema for his valuable comments and criticism. I am grateful to Dr. C.S. Strom for putting her computer program CRYSTALDRAW at my disposal and for correcting the English manuscript.

References

ABU-EID, R.M. & BURNS, R.G. (1976): The effect of pressure on the degree of covalency of the cation–oxygen bond in minerals. *Amer. Mineral.* **61**, 391-397.

BAUTSCH, H.J., FANTER, D. & MELLE, G. (1971): Kristalstructurelle Ableitung der Spaltbarkeit beim Olivin. *Ber. deut. Ges. geol. Wiss. B. Mineral. Lagerstättenf.* **16**, 205-211.

BENNEMA, P. & GILMER, G.H. (1973): Kinetics of crystal growth. *In* Crystal Growth. An Introduction (P. Hartman, ed.), North-Holland, Amsterdam.

BHAGAVANTAM, S. (1955): Elastic properties of single crystals and polycrystalline aggregates. *Indian Acad. Sci. Proc.* A41, 72-90.

BIRLE, J.D., GIBBS, G.V., MOORE, P.B. & SMITH, J.V. (1968): Crystal structures of natural olivines. *Amer. Mineral.* **53**, 807-824.

BORN, L. (1964): Eine "gitterenergetische Verfeinerung" der freien Mg-Position im Olivin. *Neues Jahrb. Mineral. Monatsh.*, 81-94.

BORN, M. & HUANG, K. (1954): *Dynamical Theory of Crystal Lattices.* Clarendon, Oxford.

BROTHERS, R.N. (1959): Flow orientation of olivine *Amer. J. Sci.* **257**, 574-584.

BROWN, I.D. & SHANNON, R.D. (1973): Empirical bond-strength–bond-length curves for oxides. *Acta Cryst.* A29, 266-282.

DONALDSON, C.H. (1976): An experimental investigation of olivine morphology. *Contr. Mineral. Petrology* **57**, 187-213.

FLEET, M.E. (1974): Distortions in the coordination polyhedra of *M* site atoms in olivine, clinopyroxenes, and amphiboles. *Amer. Mineral.* **59**, 1083-1093.

——— (1975): The growth habits of olivine — a structural interpretation. *Can. Mineral.* **13**, 293-297.

GIESE, R.F., JR. (1974): Surface energy calculations for muscovite. *Nature* 248, 580-581.

GOLDSCHMIDT, V. (1920): *Atlas der Krystallformen VI. Markasit-Pyrit.* Carl Winters Universitätsbuchhandlung, Heidelberg.

'T HART, J. (1978): The structural morphology of olivine. I. A. qualitative derivation. *Can. Mineral.* **16**, 175-186.

——— & WESSICKEN, R. (1977): The morphology of cobalt olivine (Co_2SiO_4). *Neues Jahrb. Mineral. Monatsh.*, 408-413.

HARTMAN, P. (1956): An approximate calculation of attachment energies for ionic crystals. *Acta Cryst.* **9**, 569-572.

——— (1973): Structure and morphology. *In* Crystal Growth. An Introduction. (P. Hartman ed.). North-Holland, Amsterdam.

——— (1974): The crystal habit of fluorite. *In* Minerogenezis (E. Aleksiev, I. Mincheva — Stefanova & T.G. Radonova, eds.). Izd. Bulg. Nauk, Sofia.

——— & PERDOK, W.G. (1955): On the relations between structure and morphology of crystals I. *Acta Cryst.* 8, 49-52.

HINTZE, C. (1897): *Handbuch der Mineralogie II.* Veith & Co., Leipzig.

HUGGINS, M.L. & SAKAMOTO, Y. (1957): Lattice energies and other properties of crystals of alkaline earth chalcogenides. *J. Phys. Soc. Japan* **12**, 241-251.

JAHNKE, E. & EMDE, F. (1960): *Tables of Higher Functions.* B.G. Teubner Verlagsgesellschaft, Leipzig.

KALB, G. & KOCH, L. (1929): Die Kristalltracht des Olivin und Chrysoberyll in minerogenetischer Betrachtung. *Zentr. Mineral. Geol. Paläont. Abt. A*, 169-174.

KITTEL, C. (1971): *Introduction to Solid State Physics* (4th ed.), John Wiley & Sons, New York.

KLEBER, W. (1939): Die Potentiale von Ionenketten und ihre kristallographische Bedeutung. *Neues Jahrb. Mineral. Geol. Paleont. BeilBd.* A75, 72-89.

LOMBARDI, E. & JANSEN, L. (1966): Crystal stability of AX_2 compounds in terms of three-ion interactions. *Phys. Rev.* **151**, (Ser. 2), 694-709.

MADELUNG, E. (1918): Das elektrische Feld in Systemen von Regelmässig angeordneten Punktladungen. *Phys. Z.* **19**, 524-533.

NIGGLI, P. (1927): *Tabellen zur allgemeinen und speziellen Mineralogie.* Gebrüder Borntraeger, Berlin.

——— (1941): *Lehrbuch der Mineralogie und Kristallchemie* (3rd ed.). Gebrüder Borntraeger Verlag, Berlin-Zehlendorf.

——— & FAESY, K. (1921): Olivinmischkristalle. *Z. Krist.* **56**, 436-442.

OHASHI, Y. & BURNHAM, C.W. (1972): Electrostatic and repulsive energies of the *M*1 and *M*2 cation sites in pyroxenes. *J. Geophys. Res.* **77**, 5761-5766.

POVARENNYKH, A.S. (1972): *Crystal Chemical Classification of Minerals* **1**. Plenum Press, New York.

RAYMOND, M. (1971): Madelung constants for several silicates. *Carnegie Inst. Wash. Year Book* **70**, 225-227.

SCOTT, E.R.D. (1977): Formation of olivine–metal textures in pallasite meteorites. *Geochim. Cosmochim. Acta.* **41**, 693-710.

SHANNON, R.D. & PREWITT, C.T. (1969): Effective ionic radii in oxides and fluorides. *Acta Cryst.* B25, 925-946.

SLAUGHTER, M. (1966): Chemical binding in silicate minerals. III. Application of energy calculations to the prediction of silicate mineral stability. *Geochim. Cosmochim. Acta.* **30**, 323-339.

SOELLNER, J. (1911): Über Fayalit von der Insel Pantelleria. *Z. Krist.* **49**, 138-151.

STROM, C.S. (1977): CRYSTALDRAW, an interactive APL program for making crystal drawings from central distances. *Geol. Mineral. Inst. Leiden State Univ.* (unpubl.).

TOKONAMI, M., MORIMOTO, N., AKIMOTO, S., SYONO, Y. & TAKEDA, H. (1972): Stability relations between olivine, spinel and modified spinel. *Earth Planet. Sci. Lett.* **14**, 65-69.

TOSI, M.P. (1964): Cohesion of ionic solids in the Born model. *In* Solid State Physics (F. Seitz & D. Turnbull, eds.) **16**, 1-120.

VERWEY, E.J.W. (1946): Lattice structure of the surface of alkali halide crystals. *Rec. Trav. Chim. Pays Bas* **65**, 521-528.

VU TIEN, L., GRANDIN DE L'EPREVIER, A., GABIS, V. & ANTHONY, A.M. (1972): Amélioration de la méthode des flux, synthèse et purification d'un minéral: la forstérite. *J. Cryst. Growth.* **13/14**, 601-603.

WOENSDREGT, C.F. (1971): ENERGY, a Fortran IV program to compute surface energies in an electrostatic point charge model. *Geol. Mineral. Inst. Leiden State Univ.* (unpubl.).

WULFF, G. (1901): Zur Frage der Geschwindigkeit des Wachsthums und der Auflösung der Krystallflächen. *Z. Krist. Mineral.* **34**, 449-530.

ZAMBONINI, F. (1900): Ueber den Olivin Latiums. *Z. Krist. Mineral.* **32**, 152-156.

——— (1905): Über einige Mineralien von Canale Monterano in der Provinz Rom. *Z. Krist. Mineral.* **40**, 49-68.

Received January 1978; revised manuscript accepted July 1978.

APPENDIX

For materials with a halite structure it is rather simple to compute almost exactly the total repulsion energy per molecule (Born & Huang 1954, Tosi 1964, Kittel 1971). For forsterite, however, the situation is much more complicated, because here we have three different types of ions, Mg^{2+}, Si^{4+} and O^{2-}. Furthermore, only one-half of the octahedral voids and one-eighth of the tetrahedral voids in the forsterite structure are occupied. This is in contrast with the halite structure, where all the octahedral voids and none of the tetrahedral voids are occupied.

Because we have three types of ions, we can expect repulsive forces between Si–O, Mg–O, O–O, Mg–Mg, Si–Si and Mg–Si atoms. Only the first three distances represent nearest neighbors and they will be considered as contacts primarily contributing to the repulsion energy.

The problem, however, is that Born repulsion energy of alkali halides has been computed on the basis of compressibility data, which have been obtained from homogeneous elastic compression. In other words it has been assumed that owing to a certain stress all types of bonds are reduced in length by the same amount. However, the bonds considered here do not all experience the same repulsive forces.

Raymond (1971) computed a repulsion energy of about 1410 kcal/mol for forsterite, but his calculation was based on homogeneous elastic compression. Tokonami *et al.* (1972) computed a repulsion energy of 716.34 kcal/mol for cobalt olivine (Co_2SiO_4) by the method of Huggins & Sakamoto (1957).

In our case we are especially interested in the repulsion energy per contact. A crystallizing particle attached to a certain crystal face undergoes a repulsive interaction with that face and especially with the nearest neighbors to which it will be attached. The repulsion energy, which contributes to the attachment energy, is determined by the Mg–O and O–O contacts that will be formed when a molecule is attached to a crystal face. The Si–O and O–O contacts within the SiO_4 tetrahedra have no influence on the attachment energy, because none of them is assumed to be formed during the crystallization process.

At first the repulsion energy for periclase (MgO) was computed by two different methods (Born & Huang 1954, Huggins & Sakamoto 1957). In the first method the repulsion energy may be represented (Ohashi & Burnham 1972) by

$$E_{rep} = \Sigma_{ij}\, \lambda_{ij} \exp\,(-\, r_{ij}/\rho) \qquad \text{(A1)}$$

where ρ is the hardness parameter computed from equation (*A*3), r_{ij} is the distance between the *i*th and the *j*th ions and λ is the repulsion range parameter (Kittel 1971):

$$\lambda = \rho A\,(ze)^2/nr_o^2 \exp\,(-\, r_o/\rho) \qquad \text{(A2)}$$

where $A = -1.7476$, the Madelung constant for periclase, $r_o = 2.106$ Å, the nearest-neighbor distance and n is the number of nearest neighbors. It was assumed that the compliances $s_{11} = 0.408$, $s_{44} = 0.676$ and $s_{12} = -0.095 \times 10^{-12}$ cm²/dyn (Bhagavantam 1955) were measured for homogeneous elastic compression, so $\beta = 0.654 \times 10^{-12}$ cm²/dyn. From

$$r_o/\rho = 2 - \left(9V_{mol}/\beta \quad \frac{A}{r_o}\right) \qquad \text{(A3)}$$

we found $r_o/\rho = 5.356$ and $\rho = 0.39$ Å^{-1}. Now we can substitute ρ in eq. (A2) and we find $\lambda = 5.228 \times 10^{-10}$ erg/mol. According to eq. (A1) we find for the repulsion energy of periclase 203.94 kcal/mol, which is 33.99 kcal for one Mg–O bond if we assume that all the repulsion energy is due to these bonds. This is in good agreement with Huggins & Sakamoto (1957). The disadvantage of this method is the assumption that all the repulsion energy per molecule is contributed by one type of bond. In a structure like that of olivine, probably more types of bonds contribute to the repulsion energy. For that reason method B should be used. However, this method gives no satisfactory results for Si–O bonds, which have a high repulsion energy

per bond. But because only Mg–O and O–O contacts were considered to influence the attachment energy, this method may be applied in our case. According to Huggins & Sakamoto (1957), the repulsion energy for one molecule is

$$E_{rep} = b \sum_{ij} c_{ij} \exp [a(r_i + r_j - r_{ij})] \qquad (A4)$$

where E_{rep} is the total repulsion energy of all the bonds considered for one molecule and $b = 10^{-12}$ erg is a conversion factor. The factor c_{ij} (Pauling's coefficient) gives roughly the dependence of the overlap repulsion energy between two ions on their valences and on the number of electrons in the outermost shells. In $c_{ij} = 1 + (z_i/n_i) + (z_j/n_j)$, z_i and n_i are respectively valence and number of electrons in the outermost shell of the ith ion. So $c_{Mg-O} = 1$, $c_{O-O} = 0.5$. The repulsion constant $a = 1/\rho$ is 2.56 for Mg–O bonds if we take $\rho = 0.39$, as we found for periclase and $a = 1.79$ for O–O contacts computed from the O–O distances in periclase ($r_{O-O} = 2.978$Å, $r_O/\rho = 5.356$ and $\rho = 0.56$); r_{ij} is the distance between the two nearest neighbors and r_i and r_j the effective repulsion radii. All the parameters are known, except r_i and r_j. The effective repulsion radius of oxygen is considered to be 1.38Å (Shannon & Prewitt 1969, Tokonami *et al.* 1972). The effective repulsion radius $r_{Mg} = 1.01$Å now could be computed from the periclase structure, because both methods should give the same repulsion energy.

We made the assumption that the same parameters could be used for both periclase and olivine for the Mg–O and O–O repulsion. This seems a reasonable assumption, because in both minerals the distances within the MgO_6 octahedra are quite comparable. It has been shown that the repulsion energy within the MgO_6 octahedra is nearly the same for different minerals. Huggins & Sakamoto (1957) computed for periclase 202 and 170 kcal/mol for two different repulsion parameters. For olivine Born (1964) found 262.5 kcal per MgO_6 octahedron to be the minimum for the Mg–O repulsion, and Ohashi & Burnham (1972) found for the $M(1)$ sites of different pyroxenes 204.0–225.5 kcal per octahedron.

From projections of the crystal structure of forsterite ('t Hart 1978, Figs. 2–5), it is possible to determine which Mg–O and O–O contacts have to be considered for the different F faces. The contribution of these contacts to the repulsion energy for the different faces is given in Table 5 (deposited). There is a big difference between the two models because in the last one the O–O contacts are also taken into account. However, the total contribution for the different faces per molecule is quite comparable. In Table 1 we see for the three different models the influence of the repulsion energies on the attachment energies, computed according to Huggins & Sakamoto (1957). There $E''_{att} = E'_{att} - E_{rep}$. It seems unrealistic not to consider O–O repulsion. Firstly, oxygen ions have large ionic radii, and secondly, a large number of O–O contacts will be formed by the attachment of a crystallizing particle on a crystal face.